Additive Manufacturing Letters 8 (2024) 100187

Contents lists available at ScienceDirect

Additive Manufacturing Letters

journal homepage: www.elsevier.com/locate/addlet

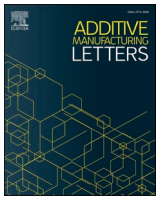

Short Communication

Powder sheets additive manufacturing: Principles and capabilities for multi-material printing

Wenyou Zhang [a,*], Arnoldas Sasnauskas [a], Asli Coban [b], Silvia Marola [c], Riccardo Casati [c], Shuo Yin [a], Ramesh Padamati Babu [b,*], Rocco Lupoi [a,*]

[a] Trinity College Dublin, The University of Dublin, Department of Mechanical, Manufacturing & Biomedical Engineering, Dublin, Ireland
[b] Trinity College Dublin, The University of Dublin, School of Chemistry, CRANN & AMBER, Dublin, Ireland
[c] Department of Mechanical Engineering, Politecnico di Milano, Via G. La Masa 1, 20156 Milan, Italy

ARTICLE INFO

Keywords:
Powder sheets
Multi-material composites
Printability
Defect-free
Additive manufacturing

ABSTRACT

In this work, a novel Metal Additive Manufacturing using Powder sheets (MAPS) method for printing multi-material composites in one process is proposed. MAPS employs powder sheets (i.e. metal powder-polymer matrix flexible films) as the feedstock material. Its key advantages include a relatively rapid change from one material to another and a minimum wastage of materials due to the elimination of the powder bed. The powder sheets were fabricated using a 'solvent casting' method. They were then employed in a commercialised metal printer for printing metal multi-material composites. To prove the disruptive concept of MAPS, a 60-layer tri-metallic multi-material composite (304 L stainless steel, In718 and CoCrFeMnNi high entropy alloy) was additively manufactured using three different types of powder sheet material in the same manufacturing system for the first time. Experimental results indicate a high density (99.80 %) multi-material composites was printed by MAPS. EDX and SEM observations of the multi-material composites revealed variations of chemical composition and microstructure along the build direction. The newly proposed MAPS manufacturing method and results of this study provide insights into a new avenue for multi-material metallic parts.

Introduction

Compared to single-material printing, multi-material composites manufacturing holds the promises of multi-functionality, spatially tailored physical properties and a greater design freedom [1,2]. The conventional multi-material composites are typically manufactured by joining separately manufactured single-material components at the post-fabrication process, which is time consuming [3]. Laser beam powder bed fusion (PBF-LB/M) provides the capabilities of manufacturing high-quality multi-material composites in a single machine and a single step [4]. However, several inherent issues are limiting its wider applications [5–8]. 1) Depending on their individual characteristics, loose powders employed as feedstocks could cause potential safety issues such as explosion; 2) It is a labour-intensive process to switch from one form of loose powder material to another in the same PBF-LB/M system; 3) There is a high risk of material cross-contamination for multi-material composites printing, which can result in a significant amount of material wastage. In addition, it is technically difficult to manufacture multi-material composites using PBF-LB/M [3,9,10].

Therefore, novel functional manufacturing methods are needed for multi-material composites by using PBF-LB/M and a significant progress has been made in developing new systems of this kind. Wen et al. [11] invented a novel PBF-LB/M method for multi-material composites where dissimilar powders are fed via different spaces. By using this modified PBF-LB/M method, compositionally graded CoCrMo-Inconel 718 samples were successfully printed with continuous variations in the chemical compositions along the powder bed direction. Wei et al. [12] developed a hybrid technique for multi-material composites printing. The 316 L powder was spread by a blade using PBF-LB/M and Cu10Sn was deposited by an ultrasonic dispenser micro-vacuum system. A Cu10Sn copper alloy QR code was successfully printed and embedded into 316 L stainless steel components. However, for the newly developed multi-material PBF-LB/M systems, it is challenging to separate different kinds of loose powders for recycling after the fabrication processes are complete [13]. In addition, multi-material printing

* Corresponding authors.
E-mail addresses: zhangw7@tcd.ie (W. Zhang), babup@tcd.ie (R.P. Babu), lupoir@tcd.ie (R. Lupoi).

https://doi.org/10.1016/j.addlet.2023.100187
Received 7 August 2023; Received in revised form 23 November 2023; Accepted 26 November 2023
Available online 27 November 2023

by the commercialised PBF-LB/M systems is more time consuming compared to single-material printing. This is due to the long pause for cleaning that is required when changing the materials.

In this work, a novel Metal Additive Manufacturing using Powder Sheets (MAPS) method for multi-material composites is proposed. It employs a new feedstock made out of metal particles combined with a polymer (i.e. powder sheet). MAPS is a modified PBF-LB/M process that combines concepts of both PBF-LB/M and sheet lamination. Details of MAPS are shown in the Method and Materials section. Due to the elimination of loose powder, MAPS provides advantages over loose powder PBF-LB/M: 1) Functionally graded multi-material components can be printed in a single step and within a single AM system; 2) A low material consumption and a minimum wastage of powder due to easy powder sheet recycling; 3) The powder sheets are safe for storage and transportation and prevent health hazards without using the glove box; 4) The MAPS for multi-material printing can avoid the cross contamination of different materials due to the elimination of loose powder materials. For the proof of concept of MAPS, 304 L stainless steel (SS304)/In718/high-entropy alloy (HEA) multi-material composites were printed. Experimental characterisations revealed a defect-free multi-material composite was printed with variations of chemical composition and microstructure.

Method and materials

Manufacturing method

Fig. 1 illustrates the manufacturing process of MAPS. The powder sheet, which is a flexible and bendable material, is placed on the top of a base plate or the previously solidified material. It is then fed into the scanning path of a laser beam. When the laser beam is switched on, the powder binder surrounding the melt pool is vaporised or degraded due to its low boiling point. At the same time, the metal powders are melted and then solidified as the laser beam moves forward. Similar to the process of loose powder PBF-LB/M, the build platform moves down by a distance that is equivalent to one layer of thickness once the fabrication of the previous layer is complete. Following that, another fresh powder sheet is spread by rollers on the top surface of the previously solidified material (Fig. 1). This method does not need post-sintering steps to eliminate the polymer binder; polymer elimination and powder fusion take place at the same time. In MAPS, switching material for the consecutive layer is easy to operate by rotating the rollers, with which a powder sheet is incorporated within. These steps are repeated until the entire manufacturing process is complete. To switch the powder sheet material being used, the previous flexible powder sheet is removed, followed by the installation of a new powder sheet material which is incorporated within the same roller.

Unlike metal laminated object manufacturing (LOM) or sheet lamination, which employs metallic foils/sheets as feedstocks, MAPS utilises loose powder-polymer binder composite as raw material. In LOM, laser cutting is needed to cut the feedstocks into a designed shape and then glue/heat/ultrasonic is typically used to bond materials between adjacent layers [14]. Thus, the precision and surface finish of LOM manufactured metallics are lower than those manufactured by other AM methods. In MAPS, due to the usage of loose powder, the precision and surface finish are expected to be comparable to that of PBF-LB/M and are higher than the LOM.

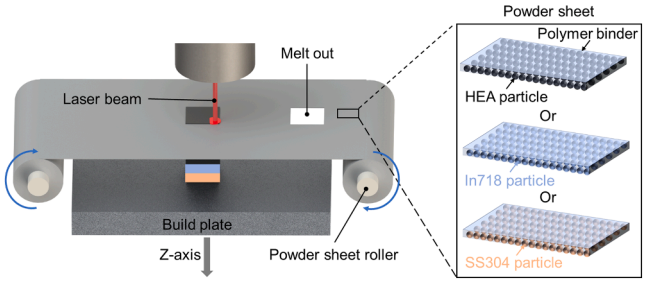

Fig. 1. Schematic illustration of MAPS manufacturing process by using different metal powder sheets.

Powder sheet manufacturing

To prepare the solution for making the powder sheets, Polycaprolactone (PCL, $(C_6H_{10}O_2)_n$) pellets with a density of 1.145 g/cm^3 were firstly dissolved in $CHCl_3$ [15]. This was followed by mixing the pre-solution (PCL and $CHCl_3$) with metal powder. In this work, three different metal materials were applied, namely SS304 (Carpenter Additive, powder size of 15–45 μm), In718 (Höganäs, 15–45 μm) and CoCrFeMnNi high entropy alloy (H. C. Starck, 15–60 μm). The scanning electron microscope (SEM, Zeiss ULTRA plus) morphologies and X-ray diffraction (XRD, Bruker D8 Discovery) patterns of each of the three loose powders are shown in Fig. 2. The XRD pattern indicates a typical single-phase face-centered cubic (FCC) crystal structure for all the three materials, which could form a good cohesive interface between any two of the three materials [16]. A comparison of the corresponding chemical compositions is shown in Table 1. The metal-polymer-solvent mixture was poured on a flexible Teflon sheet. A doctor blade (i.e. coating blade), which is 90° bevelled compared with the Teflon sheet, is then moved at a constant speed of 5 cm/min and the solvent evaporates from the mixture, leaving the metal powder and polymer to solidify. This forms a composite film. Finally, the solidified metal-polymer composite film was peeled off from the Teflon sheet and was then employed in MAPS.

Metal parts manufacturing

The multi-material sample was manufactured by a commercial Realizer SLM50 PBF-LB/M system in the AMBER AR-Lab in TCD. A continuous-wave (CW) fibre laser beam with a spot diameter of 70 μm ($1/e^2$ of the Gaussian profile) was employed. The print was performed under an argon atmosphere with a gas flow speed of 85 L/min. The machine was modified to allow for MAPS processing (the powder recoater was removed, and laser parameters adjusted). To explore the printability of powder sheets and to characterise the performance of the printed multi-material sample, 20 layers of a Ø5 mm SS304 cylinder was firstly printed. This was followed by 20 layers of In718 and then 20 layers of CoCrFeMnNi HEA, as shown in Fig. 1. The thickness of the powder sheet was measured by a Laserliner (CoatingTest-Master) apparatus. This measurement was reported as 117±5 μm (SS304), 76±8 μm (In718) and 138±9 μm (HEA), respectively. The sample was manufactured using a laser power of 100 W (which is the maximum power of the Realizer SLM 50 printer) and a scanning speed of 300 mm/s. The main purpose of this study is to check if the MAPS concept is suitable for multi-material composites printing. Thus, three materials with similar physical properties are applied, and thus the same process parameters are used. The commonly used hatch spacing of 100 μm and 90° layer rotation of unidirectional scanning strategy were employed for multi-material printing using powder sheets [5].

With regards to the printing processes of multi-material composites, the SS304 powder sheet was placed directly above a stainless steel base plate. The laser beam was then switched on and it scanned the powder sheet by following the pre-defined scanning path of the 3D model. After finishing printing of one layer, the base plate was lowered by one layer's thickness. Before printing the next layer, the powder sheet was moved horizontally to ensure that a fresh piece of powder sheet was placed above the area to be sintered. The laser beam was then switched on once again to manufacture the next layer. The roller system design shown in Fig. 1 is still a work in progress. Thus, for the preliminary test, the positioning of the powder sheet over the base plate was manually changed for printing of the next layer (this is operated via a glove-box installed in the process chamber). For the multi-material printing, after finishing the fabrication of 20 layers of SS304, the In718 powder sheet was then used for printing of the intermediate 20 layers, followed

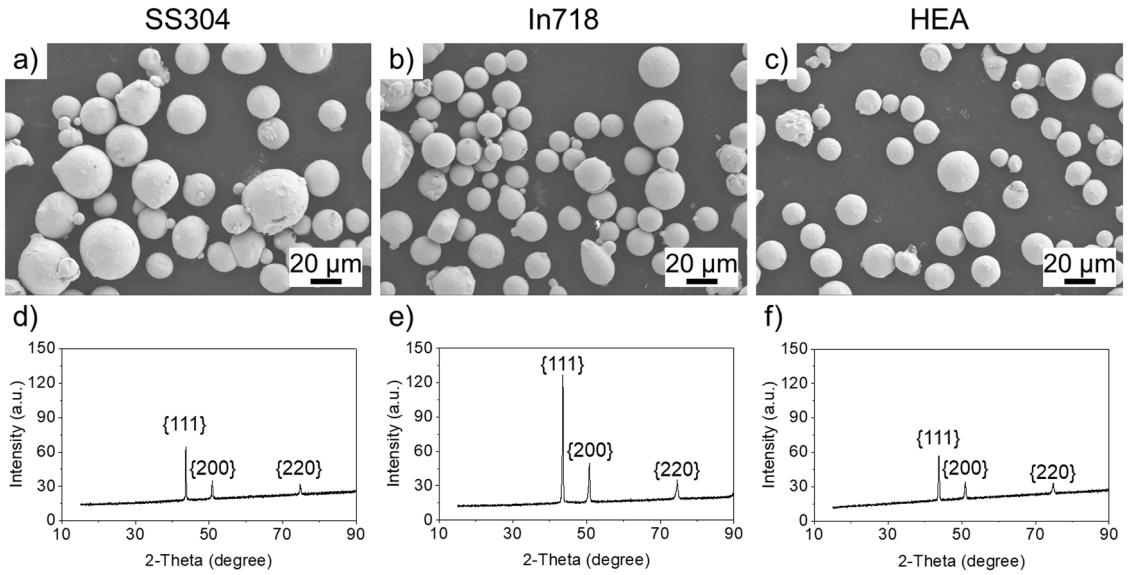

Fig. 2. Characterisations of loose powders (SS304, In718 and CoCrFeMnNi HEA) used for fabricating powder sheets: a) to c) SEM observation; d) to f) XRD pattern.

Table 1
Composition analysis and comparison of SS304, In718 and CoCrFeMnNi HEA loose powders (wt%).

	Si	Cr	Ni	Mn	C	O	S	P	Fe	Co	Mo	Ti	Nb+Ta
SS304	0.66	18.4	9.2	1.2	0.028	0.03	0.005	0.04	Bal.				
In718		18.2	53						Bal.	0.98	2.8	1.1	5.2
CoCrFeMnNi HEA		18.2	21.2	17.9					19.5	Bal.			

finally by printing 20 layers using the CoCrFeMnNi HEA powder sheet.

All the powder sheets were placed in the printing chamber before commencing the manufacturing process. Changing the material is realised by operating the glove box, ensuring the process takes place in an inert gas environment. To change the powder sheet materials, the printing chamber is opened. There is roughly a 10-minute interval between finishing printing of the first material and beginning printing of the second material. With the final automatic setup, material change will be operated in few seconds.

Material characterisation

After being manufactured, the multi-material sample was cut by using wire electric discharge machining (Excetek V440G EDM) to characterise its cross-section. The as-built sample was first mounted, followed by grinding using abrasive sandpapers. The sample was then sequentially polished by diamond suspensions of 6 μm, 3 μm, and 1 μm, respectively. This was followed by a 0.25 μm silica polishing step. Energy-dispersive X-ray spectroscopy (EDX) analysis was performed on the polished multi-material print. Based on the cross-section OM images of the polished sample, the area fraction of pores of the multi-material sample was measured by using ImageJ software. The relative porosity was calculated as the percentage of the pixels of pores over the total number of pixels of the OM image, following the methods in [17]. Finally, to clearly see the microstructure of the sample, the polished sample was electrochemically etched by using a reagent of 69 % nitric acid and 31 % water while applying a 2 V DC current [18]. SEM was then used for microstructural analysis along the cross-section of the etched samples. Thermogravimetric analysis (TGA) of the SS304, In718 and CoCrFeMnNi HEA powder sheets was performed under a nitrogen environment, with the powder sheets heated from 30 to 800 °C at a heating rate of 10 °C/min.

Results and discussion

Powder sheets characterisations

SEM observations of the raw SS304, In718 and HEA powder sheets indicate that the polymer binder connects the metal particles tightly and evenly (Fig. 3a). It is interesting to see that all of the fabricated powder sheets have two different sides: a “metal particle side” and a “polymer binder side”. This phenomenon can have different explanations. It could be attributed to the drying of the casted powder sheets, proceeding from top to bottom since the solvent initially evaporates at the top surface. The meniscus begins to withdraw towards the inner section of the powder sheets as liquid is carried to the top side by capillary forces [15, 19]. Due to that effect, the optical properties of the polymer binder and metal particle sides of the powder sheets are different. The heat transfer, polymer evaporation, and energy that the feedstocks absorb to melt the materials can therefore be altered by placing different sides of the powder sheet (i.e. polymer binder or metal particles) to be in direct contact with the base plate. In the experiments, the authors found that it is advantageous to place the “metal particle side” face down with respect to the build plate during MAPS processing. This is due to the fact that it is easier for the gas to be evaporated.

To determine the thermal decomposition of the PCL polymer binder, TGA analysis was carried out with SS304/In718/HEA powder sheets placed in a nitrogen atmosphere. Fig. 3b shows that the decomposition temperatures of the three powder sheets differ with each other, due to different packing densities caused by different physical properties such as densities of the loose powders. The TGA results show that only metal powders exist when the temperature is higher than 400 °C. For reference, 95.72 %, 92.14 %, and 95.96 % of the material in the powder sheets is SS304, In718 and HEA powder by weight respectively.

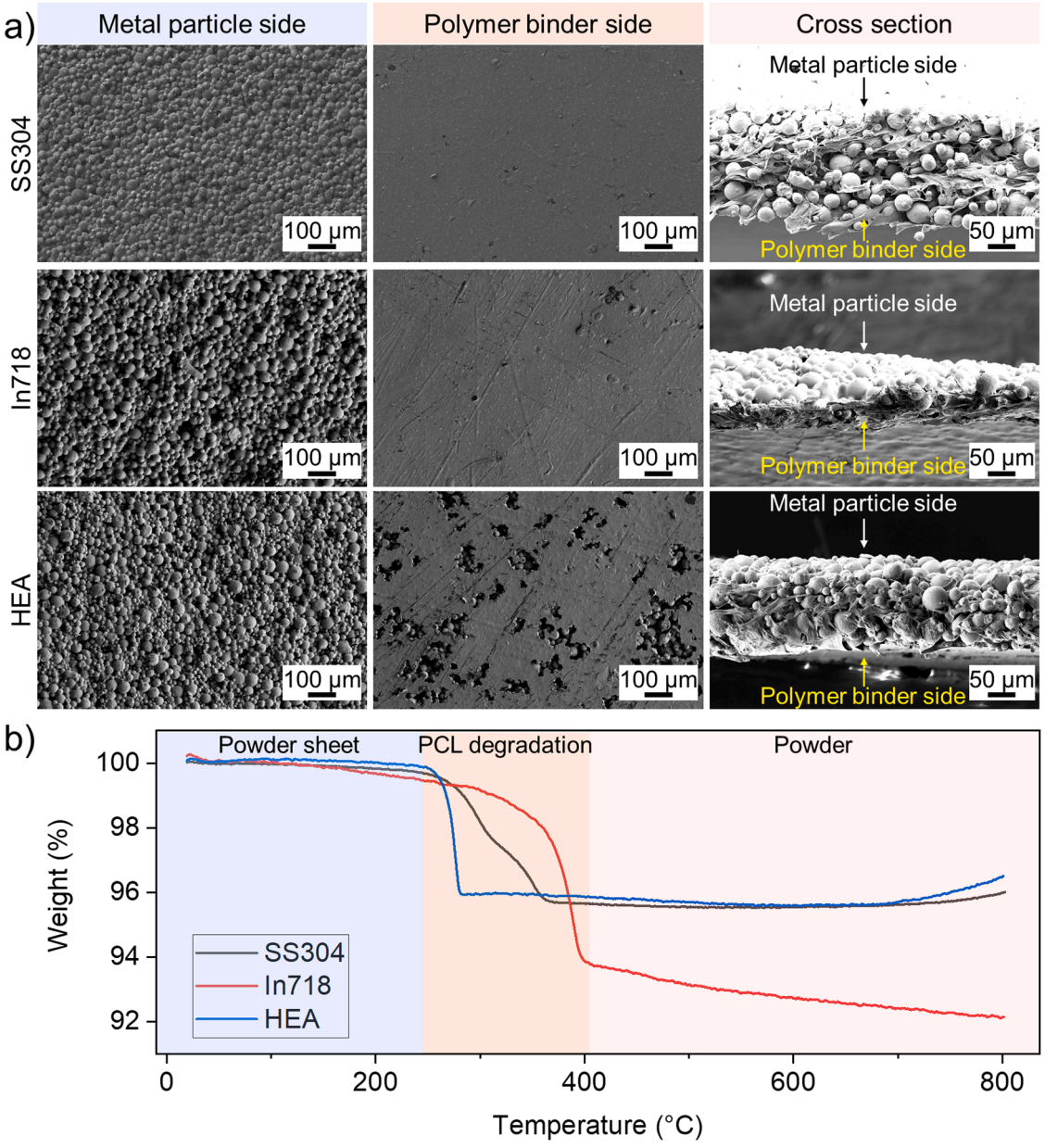

Fig. 3. Characterisations of SS304, In718 and HEA powder sheets: SEM observations (a) and TGA (b).

MAPS multi-material characterisations

Fig. 4a shows the overall view of the MAPS printed SS304/In718/CoCrFeMnNi HEA sample. Optimisation of the "edge effect" [20] of MAPS printed multi-material composites will be performed in the further works.The EDX map of the multi-material sample is shown in Fig. 4b. The EDX mapping results revealed compositional transitions between these three materials and defect-free interfaces were achieved. No cracks or defects were found at either the HEA-In718 interface (composition gradient material zone, CGZ1) or the In718-SS304 interface (CGZ2). A nearly fully dense multi-material sample (99.80 % of the relative density) was printed by using MAPS (Fig. 4a); post-sintering steps (such as those necessary in binder jetting techniques) were not applied. This is one of the key aspects of MAPS, which differentiates it from other AM methods.

XRD results (Fig. 4d) show that there is no apparent difference between MAPS printed HEA and the virgin loose powder, as an example, there is no significant difference in locations of peaks from the XRD analysis. The content of O, N and H within MAPS printed SS304 was experimentally measured by a LECO elementary analyser and compared with those of PBF-LB/M. Elemental analysis results (Table 2) confirm that there are low N, O and H residuals in the MAPS printed sample, compared to those of PBF-LB/M printed SS304.

The line EDX analysis of the SS304-In718-HEA multi-material print is shown in Fig. 4c. A gradual change in the composition can be found in the transition areas (CGZ1 and CGZ2). For the CGZ1, the interfacial region consists of a fusion zone with intermixed fused Ni, Mn, and Co. While the interfacial region of CGZ2 consists of a fusion zone with intermixed fused Fe and Ni. The same phenomenon was found in another loose powder PBF-LB/M study [21]. The formation of the CGZs (or dilutions) is caused by deposition of one metal material over another and remelting of the material resulted in a mixture of compositions at the transition areas [21]. For the MAPS printed multi-material sample, the thickness of the CGZ1 and CGZ2 is ~ 50 μm and ~ 80 μm respectively. This indicated strong interfacial bonding was formed at CGZ1 and CGZ2, despite the different properties of these three metallic materials.

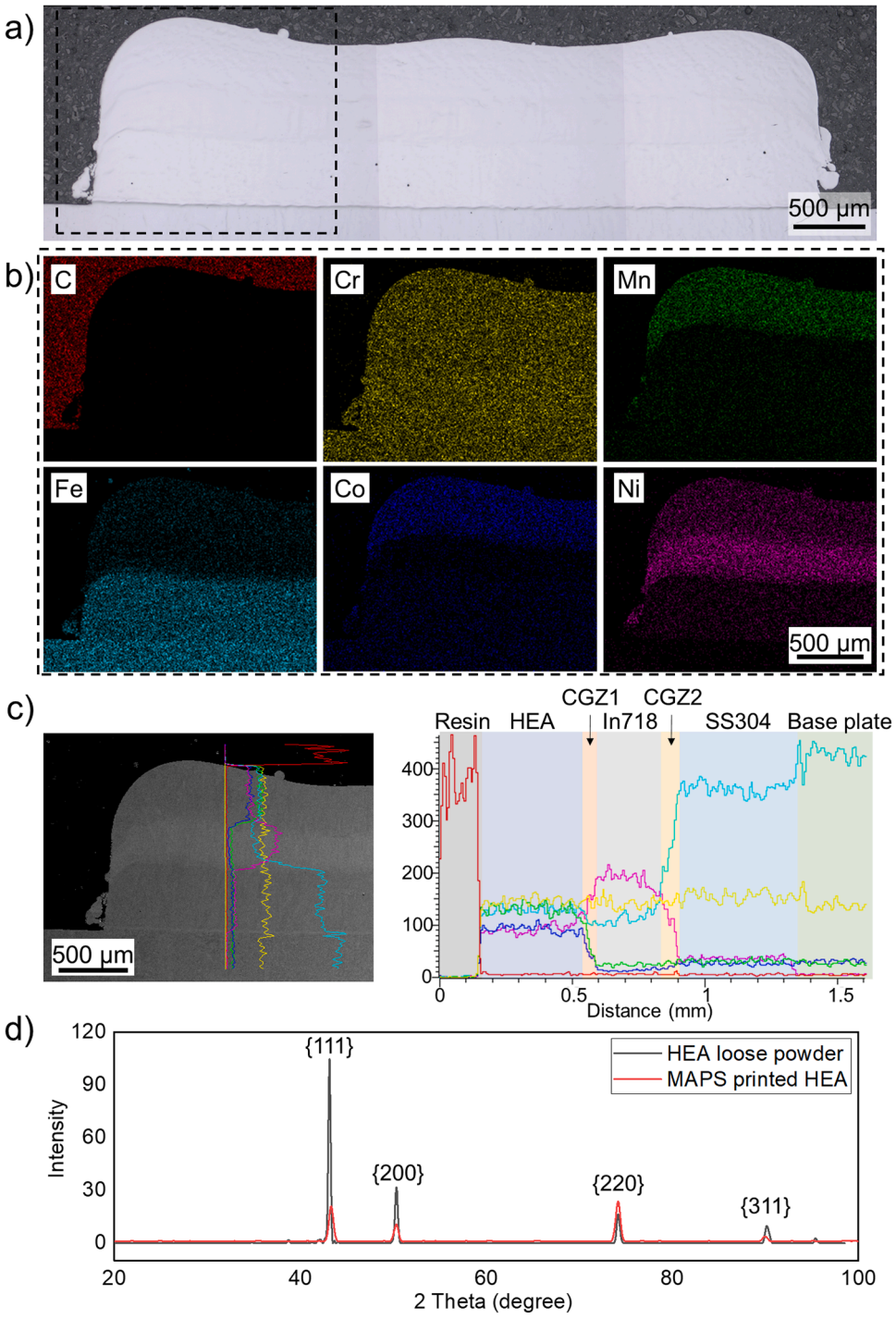

Fig. 4. Light microscopy (a) and EDX of SS304-In718-CoCrFeMnNi HEA multi-material composites: EDX map (b) and EDX line (c) analysis of multi-material composites along the build direction; XRD comparison of MAPS printed HEA and virgin HEA loose powder (d).

Table 2
Elemental contents in MAPS and PBF-LB/M printed SS304 samples.

	N (wt.%)	O (wt.%)	H (ppm)
PBF-LB/M	0.063	0.031	5
MAPS	0.058	0.017	23

In addition, the average layer thickness of the solidified material is ~23 μm, ~13 μm, and ~20 μm for the SS304 (at the bottom section), In718 (at the middle section) and HEA (at the top section), respectively. This is induced by the difference in the thickness and the powder packing densities of the three powder sheets.

Fig. 5a–f shows the microstructure of three different materials (SS304, In718 and HEA) and transition zones (CGZ1 and CGZ2, Fig. 4) along the cross-section after etching of multi-material composites, respectively. A hierarchical microstructure was observed in the trimetallic sample due to the layer-to-layer heating-melting-cooling-solidification processes of MAPS [22]. The overall SEM observation of the multi-material is shown in Fig. 5a, which shows cellular-dendritic microstructures throughout all the investigated layers. Fig. 5b shows that a shallow melt pool feature was formed for the top section of HEA

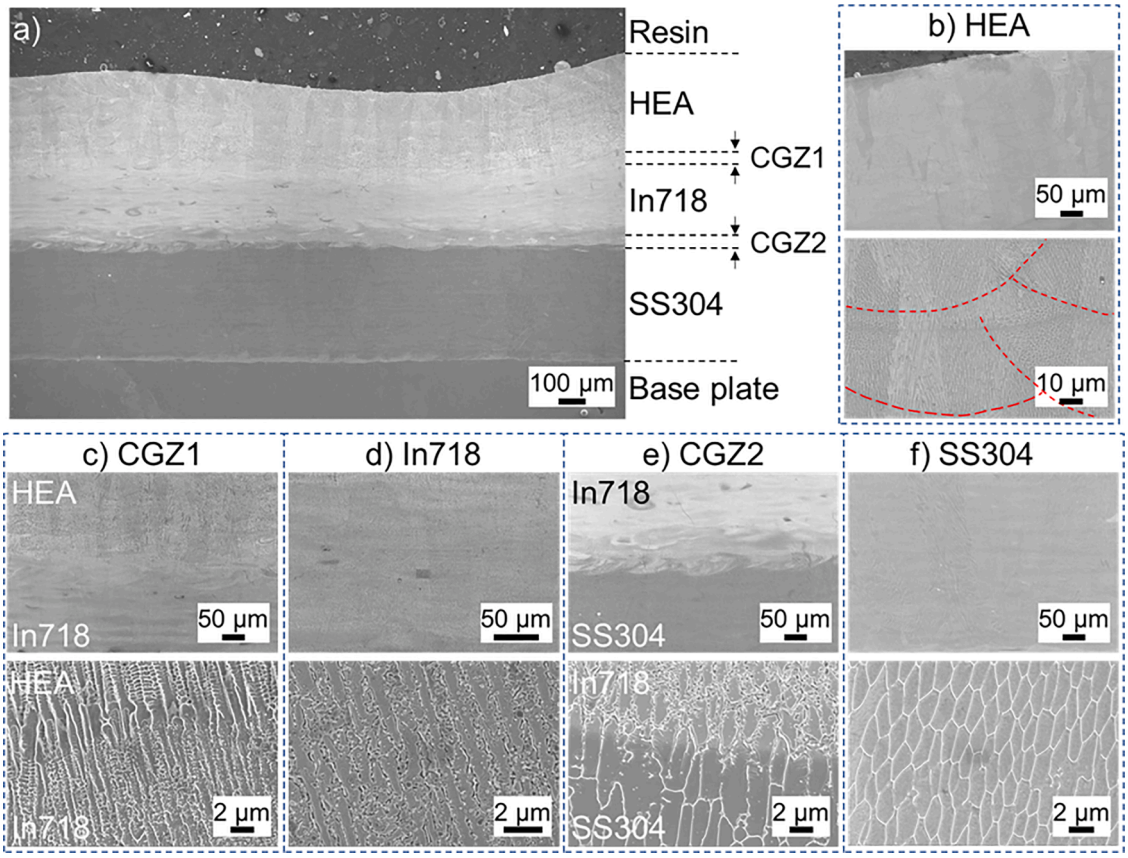

Fig. 5. Cross section SEM observation of etched microstructure (a-f) of multi-material print by using powder sheets feedstock.

material, representing the conduction mode (similarly with that of the loose powder PBF-LB/M [23]). Fig. 5c and e indicate the microstructure at the interfaces (i.e. heat affect zones) between two materials, with finer cellular sub-structures at the middle In718 layers (less than 1 μm) than the bottom SS304 and top HEA layers (2 μm). For the deposited SS304, fine cellular structures were formed within the melt pool (Fig. 5f), which is in line with those of the loose powder PBF-LB/M [24,25]. Progressions in chemical composition (Fig. 4c) and microstructural features (Fig. 5a–f) illustrate that metallurgical bonding was achieved at the interface between each of the two materials.

In this work, defect-free multi-material composites printed by using a newly proposed MAPS technique are achieved. To optimise the MAPS printing for multi-material composites, there are several further works to perform: 1) MAPS is expected to avoid cross contamination of materials, thus, the un-sintered powder sheets can be recycled. In future, the effect of materials recycling on the characterisation of MAPS printed multi-material samples should be investigated; 2) Exploring the optimum configurations for printing multi-material composites with complex geometries such as overhang structure. With an appropriate machine design, the direction of print can be moved spatially, in a way like the directed energy deposition AM, due to that polymer binder connects the metallic powder tightly. 3) To measure residual stress and bonding strength of the MAPS printed multi-material components, especially when using the optimum printing configurations for different metallic materials.

Conclusions

A novel Additive Manufacturing concept (MAPS) for printing multi-material components is proposed. In MAPS, the powder bed is eliminated and replaced by a composite sheet material made out of metallic powder and a polymer, which makes the feedstock material safer to handle. The new powder sheet printing technique can significantly improve the materials' switchover efficiency, provide more freedom to control the flexibility of feedstock, and avoid cross-contamination of materials. Three different powder sheets were fabricated by using a 'solvent casting' method. A nearly fully dense (99.80 % of relative density) cylindrical structure was successfully printed by using three different metal materials (SS304-In718-CoCrFeMnNi HEA) stacked up in layers for the first time. Post-sintering for densification (such as in binder jetting) was not needed; the prints are of high density as made. The EDX mapping and SEM results revealed a defect-free bonding and an appropriate chemical composition transition between materials, without the necessity of post-sintering steps. Microstructural observations showed a gradient variation of interphases along the build direction of the multi-material print. Elemental analysis confirms that there are no N, O and H contaminations in the MAPS printed SS304 samples. This work provides a new solution for multi-material functionally graded components in AM.

CRediT authorship contribution statement

Wenyou Zhang: Conceptualization, Investigation, Methodology, Writing – original draft. **Arnoldas Sasnauskas:** Investigation. **Asli Coban:** Investigation. **Silvia Marola:** Investigation, Writing – original draft. **Riccardo Casati:** Validation, Writing – review & editing. **Shuo Yin:** Writing – review & editing. **Ramesh Padamati Babu:** Funding acquisition, Writing – review & editing. **Rocco Lupoi:** Funding acquisition, Conceptualization, Writing – review & editing.

Declaration of Competing Interest

The authors declare that they have no known competing financial interests or personal relationships that could have appeared to influence

the work reported in this paper.

Data availability

Data will be made available on request.

Acknowledgements

This work was financially supported by PoSAddive – Powder Sheet Additive Manufacturing (EIT RawMaterials, No. 22021), Enterprise Ireland (grant number: CF-2020-1564-A/B), Science Foundation Ireland (grant number:18/EPSRC-CDT/3581), the Engineering and Physical Sciences Research Council (grant number EP/S023259/1), and MICS (Made in Italy – Circular and Sustainable) Extended Partnership and received funding from Next-GenerationEU (Italian PNRR – M4 C2, Invest 1.3 – D.D. 1551.11-10- 2022, PE00000004). We acknowledge the technical contribution of Bobby Gillham from TCD, John Enright and Alex Conway from Irish Manufacturing Research (IMR).

References

[1] B. Rankouhi, Z. Islam, F.E. Pfefferkorn, D.J. Thoma, Characterization of multi-material 316L-Hastelloy X fabricated via laser powder-bed fusion, Mater. Sci. Eng.: A 837 (2022), 142749.
[2] M. Oel, J. Rossmann, B. Bode, I. Meyer, T. Ehlers, C.M. Hackl, R. Lachmayer, Multi-material laser powder bed fusion additive manufacturing of concentrated wound stator teeth, Addit. Manufact. Lett. 7 (2023), 100165.
[3] A. Bandyopadhyay, B. Heer, Additive manufacturing of multi-material structures, Mater. Sci. Eng.: R: Rep. 129 (2018) 1–16.
[4] X. Tian, L. Wu, D. Gu, S. Yuan, Y. Zhao, X. Li, L. Ouyang, B. Song, T. Gao, J. He, X. Lin, F. Lin, J. Zhu, D. Li, Roadmap for additive manufacturing: toward intellectualization and industrialization, Chin. J. Mech. Eng.: Addit. Manufact. Front. 1 (1) (2022), 100014.
[5] W. Zhang, M. Tong, N.M. Harrison, Scanning strategies effect on temperature, residual stress and deformation by multi-laser beam powder bed fusion manufacturing, Addit. Manufact. 36 (2020), 101507.
[6] W. Zhang, M. Tong, N.M. Harrison, Resolution, energy and time dependency on layer scaling in finite element modelling of laser beam powder bed fusion additive manufacturing, Addit. Manufact. 28 (2019) 610–620.
[7] J. Persad, S. Rocke, Multi-material 3D printed electronic assemblies: a review, Result. Eng. 16 (2022), 100730.
[8] E. Sadeghi, P. Karimi, R. Esmaeilizadeh, F. Berto, S. Shao, J. Moverare, E. Toyserkani, N. Shamsaei, A state-of-the-art review on fatigue performance of powder bed fusion-built alloy 718, Prog. Mater Sci. 133 (2023), 101066.
[9] S.C. Bodner, K. Hlushko, L.T.G. van de Vorst, M. Meindlhumer, J. Todt, M. A. Nielsen, J.W. Hooijmans, J.J. Saurwalt, S. Mirzaei, J. Keckes, Graded Inconel-stainless steel multi-material structure by inter- and intralayer variation of metal alloys, J. Mater. Res. Technol. 21 (2022) 4846–4859.
[10] W. Zhang, D. Guo, L. Wang, C.M. Davies, W. Mirihanage, M. Tong, N.M. Harrison, X-ray diffraction measurements and computational prediction of residual stress mitigation scanning strategies in powder bed fusion additive manufacturing, Addit. Manufact. 61 (2023), 103275.
[11] Y. Wen, B. Zhang, R.L. Narayan, P. Wang, X. Song, H. Zhao, U. Ramamurty, X. Qu, Laser powder bed fusion of compositionally graded CoCrMo-Inconel 718, Addit. Manufact. 40 (2021), 101926.
[12] C. Wei, Z. Sun, Y. Huang, L. Li, Embedding anti-counterfeiting features in metallic components via multiple material additive manufacturing, Addit. Manufact. 24 (2018) 1–12.
[13] A. Mussatto, Research progress in multi-material laser-powder bed fusion additive manufacturing: a review of the state-of-the-art techniques for depositing multiple powders with spatial selectivity in a single layer, Result. Eng. 16 (2022), 100769.
[14] Y. Shen, Y. Li, C. Chen, H.-L. Tsai, 3D printing of large, complex metallic glass structures, Mater. Des. 117 (2017) 213–222.
[15] R. Lupoi, W.M. Abbott, R. Senthamaraikannan, S. McConnell, J. Connolly, S. Yin, R.B. Padamati, Metal additive manufacturing via a novel composite material using powder and polymers formed in sheets, CIRP Ann. 17 (2022) 181–184.
[16] M.S. Duval-Chaneac, N. Gao, R.H.U. Khan, M. Giles, K. Georgilas, X. Zhao, P.A. S. Reed, Fatigue crack growth in IN718/316 L multi-materials layered structures fabricated by laser powder bed fusion, Int. J. Fatig. 152 (2021), 106454.
[17] T. Ronneberg, C.M. Davies, P.A. Hooper, Revealing relationships between porosity, microstructure and mechanical properties of laser powder bed fusion 316 L stainless steel through heat treatment, Mater. Des. 189 (2020), 108481.
[18] S. Yin, X. Yan, R. Jenkins, C. Chen, M. Kazasidis, M. Liu, M. Kuang, R. Lupoi, Hybrid additive manufacture of 316 L stainless steel with cold spray and selective laser melting: microstructure and mechanical properties, J. Mater. Process. Technol. 273 (2019), 116248.
[19] R. Riedel, I.-W. Chen, Ceramics Science and Technology, 2011.
[20] E. D'Accardi, R. Krankenhagen, A. Ulbricht, M. Pelkner, R. Pohl, D. Palumbo, U. Galietti, Capability to detect and localize typical defects of laser powder bed fusion (L-PBF) process: an experimental investigation with different non-destructive techniques, Progr. Addit. Manufact. 7 (2022) 1239–1256.
[21] M.J. Sagong, E.S. Kim, J.M. Park, G.M. Karthik, B.-J. Lee, J.-W. Cho, C.S. Lee, T. Nakano, H.S. Kim, Interface characteristics and mechanical behavior of additively manufactured multi-material of stainless steel and Inconel, Mater. Sci. Eng.: A 847 (2022), 143318.
[22] S. Min, H. Liu, M. Yang, H. Zhang, J. Hou, K. Zhang, J. Liang, J. Li, H. Wang, J. Wang, A. Huang, High-temperature oxidation performance of Ni-based GH3536 superalloy fabricated by laser powder bed fusion, npj Mater. Degrad. 6 (1) (2022) 66.
[23] M.-S. Pham, B. Dovgyy, P.A. Hooper, C.M. Gourlay, A. Piglione, The role of side-branching in microstructure development in laser powder-bed fusion, Nat. Commun. 11 (1) (2020) 749.
[24] S. Mohd Yusuf, X. Zhao, S. Yang, N. Gao, Interfacial characterisation of multi-material 316 L stainless steel/Inconel 718 fabricated by laser powder bed fusion, Mater. Lett. 284 (2021), 128928.
[25] Q. Wang, J. Chen, G. Sun, H. Liu, Z. Wang, H. Pan, Y. Zhang, P. Jiang, W. Wu, Microstructure and mechanical performance of 304 stainless steel fabricated by laser powder bed fusion: the effect of post-processing heat treatment, J. Mater. Eng. Perform. 32 (2) (2023) 695–711.